NBSIR 87-3072

Report Number 16

# CHARACTERIZATION OF RESIDUAL STRESS AND TEXTURE IN CAST STEEL RAILROAD WHEELS

A.V. Clark, Jr., H. Fukuoka,
D.V. Mitrakovic, and J.C. Moulder

U.S. DEPARTMENT OF COMMERCE
National Bureau of Standards
Institute for Materials Science and Engineering
Fracture and Deformation Division
Boulder, Colorado 80303

September 1986

Issued July 1987

Prepared for
FEDERAL RAILROAD ADMINISTRATION
Washington, D.C. 20590

NBSIR 87-3072

Report Number 16

# CHARACTERIZATION OF RESIDUAL STRESS AND TEXTURE IN CAST STEEL RAILROAD WHEELS

A.V. Clark, Jr., H. Fukuoka,
D.V. Mitrakovic, and J.C. Moulder

U.S. DEPARTMENT OF COMMERCE
National Bureau of Standards
Institute for Materials Science and Engineering
Fracture and Deformation Division
Boulder, Colorado 80303

September 1986

Issued July 1987

Prepared for
FEDERAL RAILROAD ADMINISTRATION
Washington, D.C. 20590


**U.S. DEPARTMENT OF COMMERCE, Malcolm Baldrige, *Secretary***
**NATIONAL BUREAU OF STANDARDS, Ernest Ambler, *Director***

## ADMINISTRATIVE INFORMATION

The investigation reported herein was sponsored by the Equipment and Operating Practices Safety Research Division of the Federal Railroad Administration in the Department of Transportation. The work was funded under the FRA-NBS Interagency Agreement DTFR53-84-X-00022. The technical effort was monitored by Mrs. C. Orth of the Federal Railroad Administration.

ABSTRACT

Residual stress and texture were characterized in the rim of a cast steel railroad wheel, using both an electromagnetic-acoustic transducer (EMAT) and a piezoelectric transducer. Orthogonally polarized shear-horizontal waves were propagated through the thickness of the rim, and arrival times measured (in pulse-echo) with a precision of about $10^{-5}$. The difference in arrival times (birefringence) is related to the difference of principal stresses and also to texture.

The wheel had been sawcut in a previous experiment; the residual stress had been relieved at the sawcut. The birefringence was measured at the sawcut and subtracted from the birefringence measured at stressed regions. This allowed us to map out variations in stress around the circumference of the wheel. Stresses measured with the EMAT and piezoelectric transducer agreed to within 10 MPa.

## INTRODUCTION

The presence of residual stresses in railroad wheels can be a significant factor in wheel failure. These residual stresses have two origins: (1) stresses due to fabrication of the wheel, and (2) in-service stresses induced by drag-braking. For cast steel wheels (the most common type in the US), fabrication stresses occur as the wheel cools in the mold; differential shrinkage gives rise to thermal strains (and stresses). If these stresses are above yield (for the corresponding temperature), then inhomogeneous plastic deformation results. Residual stresses are then necessary so that compatibility is satisfied; e.g., so all regions of the wheel fit together without voids, etc.

The same process that creates residual stresses on cooling also occurs (in reverse) during braking. The heat input into the tread of the wheel (region in contact with the rail) causes expansion of this region of the wheel, especially the rim. Each volume element of the rim tries to expand, but is constrained by its neighbors. Consequently, thermal expansion during braking causes a compression; if these compressive stresses exceed yield, inhomogeneous plastic deformation results. As the wheel cools after braking,

a tensile hoop stress may result to make all the regions of the rim "fit together."

We note that residual stresses due to casting will (probably) be compressive, whereas those due to excess braking will (probably) be tensile. If the latter stresses exceed the former, then the rim will be in a state of net tensile stress. Consequently, if a crack occurs in the rim, these tensile stresses can act as crack-driving forces, leading to wheel failure.

It is highly desirable to have a nondestructive testing method for measuring such residual stresses. One promising technique which has been investigated is the acoustic birefringence technique. It can be shown (both analytically and experimentally) that the presence of stress in metals induces a small velocity change (acoustoelastic effect). Subject to certain restrictions, the difference in velocity of orthogonally polarized shear-horizontal (SH) waves will be proportional to the difference of principal stresses. This (normalized) difference in velocities is called the acoustic birefringence, in analogy to the birefringence effect in photoelasticity.

Piezoelectric SH-wave transducers have been used to measure the residual stress state in Japanese rolled steel wheels [1,2]. The birefringence was measured in the as-received state (residual stresses due to rolling), after drag-braking (additional stresses due to thermal expansion), and after cutting into blocks (stress-relieved). The total residual stress (measured ultrasonically) was compared with destructive measurements; the two agreed to within 40 MPa [1,2].

In this paper, we present results of a study on the feasibility of using ultrasonics to characterize residual stress states in cast steel wheels of US

manufacture. We were interested in using electromagnetic-acoustic transducers (EMATs) for these measurements.

The EMAT has the advantage that it requires no acoustic couplant to generate sound in a metal (or other conductor). Consequently, an EMAT can be scanned, rotated, etc. over the rim of the wheel with ease. Being non-contacting, it may require less preparation of the surface (where sound is generated) than piezoelectric devices. To determine whether these potential advantages could be realized in practice, we performed a series of experiments on a cast steel wheel which had been removed from service. We measured the birefringence with an SH-wave EMAT using a simple velocity measurement system (described later). Since the birefringence method using piezoelectric transducers had been successful in determining residual stresses [1,2], we measured the birefringence using both an EMAT and a piezoelectric transducer. (In fact we used the same transducer as was used in Refs. 1 and 2.) The residual stress, as measured by both devices, was found to be in excellent agreement.

## THEORY

It can be shown that stress causes a (small) change in phase velocity in metals. Consider the case of a homogeneous, isotropic metallic plate in a state of plane stress. Let a pure-mode shear-horizontal (SH) wave be propagated through the thickness of the plate; the wave is polarized first along the $\sigma_1$ (principal stress) axis, and then along the $\sigma_2$ axis, with corresponding transit times $T_1$ and $T_2$. The acoustic birefringence, B, is defined as the normalized difference in arrival times; it is proportional to the difference of principal stress

$$B \equiv \frac{T_2 - T_1}{(1/2)(T_2 + T_1)} = C_A(\sigma_1 - \sigma_2) \tag{1a}$$

Note that since both SH-waves travel through the same material thickness,

$$B = \frac{V_1 - V_2}{(1/2)(V_1 + V_2)} \tag{1b}$$

where $V_1$ is the phase velocity of an SH-wave polarized along $\sigma_1$, etc.

The magnitude of the stress-acoustic constant, $C_A$, is rather small (about $-7.6(10^{-6})$/MPa for railroad wheels [1,2]). Consequently, the stress-induced birefringence is also small. In fact, for many common structural elements, there will be unstressed birefringence, $B_o$, due to fabrication processes (rolling, casting, etc.) which is the same magnitude as the stress-induced birefringence.

The theoretical problem of an SH-wave propagating through a slightly anisotropic body in a state of plane stress has been solved by Iwashimizu and Kubomura [3] and also by Okada [4]. For brevity, we repeat only the results of their calculations here.

It was found that pure-mode SH-waves could only be propagated when the waves were polarized along certain directions (also called acoustic axes). These axes were oriented at angle $\phi$ relative to the axes of material symmetry (to be defined later); $\phi$ is given by [3]:

$$\tan 2\phi = \frac{2 C_A \sigma_{12}}{B_o + C_A(\sigma_{11} - \sigma_{22})} \tag{2}$$

Here the normal stresses $\sigma_{11}$, $\sigma_{22}$, and the shear stress, $\sigma_{12}$, are referenced to the material symmetry axes. In the absence of shear stress, the acoustic

axes coincide with the material symmetry axes. Plane stresses are assumed in the above.

The birefringence (difference in velocity of SH-waves polarized along the acoustic axes) is given by [3]

$$B^2 = [B_o + C_A(\sigma_{11} - \sigma_{22})]^2 + (2C_A\sigma_{12})^2 \qquad (3)$$

Note that equation (3) reduces to (1) when there is no shear stress, and no unstressed birefringence.

A discussion of material symmetry axes is in order here. Normally one treats common alloys such as steel and aluminum as isotropic. However, as stated previously, processes such as rolling and casting induce a preferential orientation of the crystallographic axes of the grains (single crystals) which made up the structural elements. It is this anisotropy that gives rise to the unstressed birefringence, $B_o$. The directions of the preferential orientation are the material symmetry axes.

We note that the theory which leads to equations (2) and (3) assumes orthotropic symmetry; i.e., that any small volume element of the material has three axes of 2-fold symmetry. This assumption works quite well for rolled plates of aluminum and steel alloys. One of the purposes of our experiments was to test its validity for cast steel wheels.

## EXPERIMENT

### Railroad Wheel

A cast steel wheel, shown in Fig. 1, was obtained from the Dept. of Transportation Test Center in Pueblo, Colorado. This wheel has been removed

from service based on the "4-inch rule" [5] to prevent possible failure due to buildup of residual stresses induced by braking.[1] (If such stresses are tensile, they become crack-driving forces for any cracks existing in the wheels.)

The wheel had been sawcut as part of a test program being conducted by the American Association of Railroads for DOT. Consequently, the circumferential (hoop) stress had been relieved at the sawcut.

The wheel was milled at several locations on the front and back faces of the rim. The milled locations are indicated in Fig. 1, and a cross-section of the rim is shown in Fig. 2. The milling was done to give a smooth surface for coupling acoustic energy from a piezoelectric transducer into the wheel (as described later). No particular effort was made to make the milled surfaces plane-parallel.

In addition, other locations around the circumference of the wheel were cleaned by a variety of techniques. Some locations were merely hand-sanded to remove surface rust, leaving large pitted areas on the surface. Others were ground with a hand-grinder, and then sanded. This was done to characterize the effect of surface preparation on the velocity measurements made with electromagnetic-acoustic transducers (EMATs).

All measurements were made with the center of transducer aperture 19 mm from inner edge of the rim, as shown in Fig. 2.

Velocity Measurement System

A simple time-interval-averaging system was used for birefringence measurements; the setup used with the EMAT is shown in Fig. 3. The essentials of operation are as follows. When the pulser excites the transducer, it

---

[1]Simply put, the rule prescribes that if a band of discoloration greater than 4 inches wide forms near the rim, the wheel is to be removed.

also excites a time-interval probe which generates a TTL pulse which sends a START signal to a counter. The counter runs at 100 MHz clock rate until it receives a STOP signal. To suppress the effect of noise (a significant problem with EMAT operation), the counter can be set to average many such time intervals. We typically used an average of $10^3$ such intervals.

We wished to avoid dependence of arrival time measurements on signal amplitude. This was accomplished as follows. The received signal was amplified by a broadband receiver, followed by a high-pass filter to remove any variations in dc level with amplifier gain. The signal was then input to the STOP probe, which generates a TTL pulse when the signal reaches a selected threshold. In order to make arrival time measurements insensitive to amplitude variations, the threshold level was set to 0 volts. The output of the probe was input to a specially constructed digital delayed gate (DDG), described in more detail in the APPENDIX. In essence the DDG accomplishes the same purpose as a distortion-free analog gate, but does so by using logic circuit electronics.

The STOP probe will, of course, generate a signal each time the voltage level reaches zero. Since the EMAT system has a low signal/noise ratio, it is necessary to eliminate the STOP probe output pulses which correspond to those zero crossings generated by noise (rather than the echo received by the transducer). Typically, we set the delay on the DDG so that its output corresponded to a selected zero crossing in the r.f. echo waveform.

Velocity Measurements with EMATs

The wheel was placed in a horizontal position; since the EMAT contained a permanent magnet, no fixture was necessary to keep it in place. Measurements were made in the pulse-echo mode, with the transducers (both EMAT and

piezoelectric) placed on the back face of the rim.

The EMAT has an aperture 1 cm x 1 cm and was excited with a quasi-monochromatric tone burst having a frequency of 2.8 MHz. Arrival times were measured with the EMAT polarized in the radial (r) and circumferential ($\theta$) directions. For the cast steel wheel used here, only the first echo was useable for these measurements; the signal/noise ratio was too small for the second echo and further echoes could not be distinguished from noise on the scope trace.

Our measurements were conducted in close proximity to a welding laboratory and a laboratory equipped with mechanical testing machines (a noisy r.f. environment). Nevertheless, the precision in arrival time measurements made with our time-interval averaging system was $\pm 1$ ns (or better); since the arrival time of the first echo was approximately 90 $\mu$s, our (electronic) precision is of the order of 10 ppm. This was achieved with a signal whose amplitude (after amplification) ranged from about 200 mv to about 800 mv (zero to peak).

We observed that the signal amplitude varied with orientation; in fact, the peak amplitude was about twice as large for an SH-wave polarized in the radial direction as in the circumferential direction. Consequently, it is essential that the STOP signal to the counter be triggered by a TTL pulse (from the STOP probe) which corresponds to a zero crossing (phase = $2n\pi$) in the received r.f. waveform (1st echo).

The permanent magnet in our EMAT has a rotationally symmetric magnetic field. This is important, since it avoids the possibility that magnetic hysteresis effects could cause variations in the efficiency of converting electromagnetic energy into acoustic energy as the EMAT is rotated.

We also observed an increase in signal strength if the EMAT was left in a given location for several hours. This is possibly due to an increase in magnetic induction caused by the permanent magnet. (The amplitude of the acoustic signal is proportional to the magnitude of the applied magnetic induction in the skin depth of an electromagnetic wave incident on the wheel).

Relative velocity (birefringence) measurements were made with the EMAT polarized first in one principal stress direction (e.g. radial direction) and then in the orthogonal direction. This operation was repeated at least three times, since it was observed that arrival time measurements at the same location with the same orientation exhibited a scatter typically of the order of about 5 ns. The arrival times in each orientation were averaged, and the differences (of the two averages) were taken to give the birefringence:

$$B \equiv \frac{\langle T_r \rangle - \langle T_\theta \rangle}{1/2(\langle T_r \rangle + \langle T_\theta \rangle)} \qquad (4)$$

where $\langle T_\theta \rangle$ is the average arrival time of the SH-wave polarized in the circumferential direction, etc.

We attribute the scatter in arrival times to variations in the coupling between EMAT and wheel surface. Even though EMATS are noncontacting devices, there are effects of liftoff (distance between EMAT and surface). One effect is, of course, a decrease in the amplitude of the acoustic signal generated by the EMAT.

A second (usually smaller) effect is a phase shift (in frequency space) or an equivalent delay in the time domain. One explanation for this phenomenon is as follows. Consider the equivalent circuit for the EMAT. This

consists of the inductance of the EMAT coil, plus a complex impedance due to the electromagnetic field set up by the EMAT in the skin depth of the conductor beneath it [6]. This impedance consists of a resistance (eddy current resistance) plus an inductance. The impedance (in frequency space) has been shown to be a function of liftoff [6], so variations in liftoff will give variations in arrival times.

Variations in liftoff come from two sources in our experiments. At locations which have not been milled, there are pits remaining on the surface. Since the EMAT is not precisely registered each time it is placed on the surface, the effective liftoff varies from one placement to another.

The other source of liftoff is caused by the construction of the EMAT itself. A copper shield is placed over the front of the EMAT; the shield has an aperture 1 cm x 1 cm cut in it. (This is done to obtain a linearly polarized SH-wave). The copper shield is not flat; it has small bulges which must be flattened out by a (small) force applied to the case which houses the EMAT. To apply a constant force, we usually placed a weight on top of the EMAT case. This partially succeeded in reducing liftoff variations, but still left the previously mentioned spread of about 5 ns in arrival times.

Velocity Measurements with Piezoelectric Transducers

We wished to compare our EMAT measurements with those performed using conventional piezoelectric transducers. We used a specially made device (fabricated at Osaka University) which consists of two transducers of PZT; the transducers were oriented so that they generate orthogonally polarized SH-waves, and then one transducer was bonded on top of the other. Leads were arranged so that by throwing a switch, either the top or bottom transducer could be separately excited.

A powder backing made of copper and epoxy is bonded above the rubber to act as an acoustic absorber and increase the bandwidth of the device. A small piece of rubber was bonded to the backing material ; even if the axis of the device is not normal to the wheel surface, the transducers will have enough freedom to rotate so that they are tangent to the surface.

The piezoelectric transducer was spring-loaded to ensure a constant pressure on the viscous couplant which was used to couple a shear wave into the wheel. The device which housed the transducer and the spring was mounted on the wheel with a stand which had a magnetic base.

The electronics use to drive this stacked transducer device was different from that used to drive the EMATs; compare Figs. 3 (EMAT) and 4 (PZT). The reason for using two different arrangements is as follows.

With the PZT device, the waveforms generated by the upper and lower transducer are different; the upper transducer is "loaded" on its front face by the lower transducer, whereas, the lower transducer is "loaded" on its front face by the wheel. When using the gated amplifier (shown in Fig. 3), we could not identify corresponding zero crossings in the waveforms generated by the lower and upper transducer.

Consequently, we used a simple pulser which shock-excited the PZT transducers. By properly tuning an impedance-matching device connected between pulser and transducers it was possible to obtain clearly identifiable features in the waveforms generated by each transducer and identify the corresponding zero crossings.

We found that (for the same receiver gain) the signal received by the upper transducer was always smaller than that of the lower transducer. Furthermore, the waveforms generated by the transducers were not purely

sinusoidal. We attempted to compensate for this by changing the receiver gain so that the peak signal amplitude was the same in both waveforms.

We used the following procedure. The signal received by the lower transducer usually had a peak amplitude of about 400 mv with the (variable) receiver gain set to zero.[2] Consequently, the vertical amplifier on the oscilloscope (volts/division) was first set on 200 mv/division, and then taken out of calibration and adjusted until the peak of the waveform was two (large) units above the "ground" level (with the scope operated in the d.c. mode, rather than a.c.). The switch (shown in Fig. 4) was then thrown so that the signal from the upper transducer was received and displayed on the scope with the (uncalibrated) gain on the vertical scope amplifier unchanged, and the variable gain on the receiver was changed until the peak waveform for the upper transducer reached the same level on the oscilloscope (two large units) as that of the lower transducer. We found that this procedure seemed to result in the minimum shift in apparent arrival time with gain (about 20 ns).

Using the above procedure is a somewhat arbitrary choice, since we noted a change in apparent arrival time with receiver gain. In fact, we would expect some differences in birefringence as measured with the EMAT and the PZT transducer. With the EMATs, using a toneburst, zero crossings correspond to zero phase in the echo. For shock-excitation of the PZT transducers, which do not have a purely sinusoidal response, zero crossings do not necessarily correspond to zero phase, since a change in gain caused a change in time of zero crossing. In fact, we expect some systematic errors $\delta t_\theta$ and $\delta t_r$ in PZT arrival time measurements.

---

[2]The receiver has a fixed gain of about 30 db, plus a variable gain.

However, if we use a consistent arrival time measurement procedure, we expect that the difference between birefringence measured by EMAT and PZT will be constant. The results of our measurements seemed to bear this out, as will be shown subsequently.

Note that one advantage of the design of this stacked transducer is that couplant thickness variations are eliminated; both transducers generate SH-waves which propagate through the same couplant thickness. The arrival time of an SH-wave in the upper transducer will, of course, be increased by twice the time an SH-wave requires to propagate through the lower transducer.

To compensate for this, the arrival times for both transducers were first measured with the lower transducer polarized in the radial direction; then the (stacked) transducer was rotated 90°, and the new arrival times measured. The birefringence was calculated from

$$B \equiv 1/2[(T_r^{(\ell)} + T_r^{(u)}) - (T_\theta^{(\ell)} + T_\theta^{(u)})]/T_o \qquad (5)$$

where superscripts ($\ell$) and (u) refer to lower and upper transducers respectively; e.g., $T_r^{(\ell)}$ is the arrival time measured with the lower transducer polarized in the radial direction. $T_o$ is the average of all arrival times.

## RESULTS

### Texture Study

The theory of acoustoelasticity which led to the relations (2) and (3) was based on the assumption of orthotropic symmetry [3,4], which usually occurs in rolled plates of aluminum and steel alloys. Since we are dealing

with a cast steel wheel, it was necessary to characterize the texture (preferred orientation) to see whether the theories of Refs. 3 and 4 could be applied to our wheel.

It has been observed that for a slightly orthotropic rolled plate, the measured arrival time of an SH-wave (propagating through the plate at normal incidence) varies in a sinusoidal manner [7]. The maximum and minimum arrival times are obtained when the transducer is polarized along the acoustic axes. (For a treatment of the theory behind this effect, see Ref. 7.)

We measured the angular variations of arrival times in the sawcut wheel. Locations 1 and 2 on the wheel (adjacent to the sawcuts) have experienced a relief of hoop stress. We used our EMAT to measure the arrival time variation at location 1 as the transducer was rotated; the result is shown by the solid line in Fig. 5. The velocity is fastest for a wave polarized in the radial (r-) directions and slowest for the wave polarized in the circumferential (θ-) direction.

To be sure that the acoustic axes are oriented along radial and circumferential directions at stressed locations in the sawcut wheel, we also measured the angular variation of arrival times at location 4 (see Fig. 1). This location was 90° around the wheel circumference from the sawcuts; hence, the residual stress there should not be completely relieved by the sawcuts.

The angular variation of arrival times at location 4 is shown as the dotted line in Fig. 5; the data show that the radial and circumferential directions are still acoustic axes for stressed locations. Consequently, a necessary condition for the application of the theory of Refs. 2 and 3 has been satisfied.

Furthermore, we see that the radial and circumferential directions still appear to correspond to the fast and slow acoustic axes, respectively. The material symmetry axes still coincide with the principal stress axes, and from equation (2) the shear stress $\sigma_{r\theta}$ vanishes. The birefringence equation (3) becomes

$$B - B_o = C_A(\sigma_\theta - \sigma_r) \tag{6}$$

for the cast wheel.

The unstressed birefringence, $B_o$, was measured at locations 1 and 2 (on either side of sawcuts). The values were slightly different at each of the two locations, and were different for EMATs and the PZT transducer; see Table 1.

Table 1. Values of Unstressed Birefringence

| Location | Transducer | $B_o(10^{-4})$ |
|---|---|---|
| 1 | PZT | 7.6 |
| 2 | PZT | 6.2 |
| 1 | EMAT | 8.1 |
| 2 | EMAT | 7.4 |

We took the average of the unstressed birefringence measured at locations 1 and 2 as the value of $B_o$ to be used in equation (6); for the PZT measurements, we have $B_o = 6.9(10^{-4})$; for the EMAT, $B_o = 7.8(10^{-4})$. The difference

between these values may be due to the way arrival times are measured with the EMAT and PZT transducers, as described previously.

Birefringence Measurements

The birefringence was measured at the milled regions 1-6, using the PZT transducer. The milled surface was about 18 cm long (arc length) at each region; see Fig. 1. We measured B at least three times at each milled region. The birefringence was measured near the center of each milled region. The values of birefringence thus obtained are plotted in Fig. 6; note that the vertical axis actually equals -B since we defined $B = (T_r - T_\theta)/T_o$. The error bars represent the standard deviation of the (three or more) measurements of B at each of the 6 milled regions.

Also shown in Fig. 6 are the results of EMAT measurements on the milled surfaces. With the EMATs, we measured B at three separate locations on each milled region; we measured at the center of the milled region and at locations ± 25 mm from the center. Consequently, B was measured at a total of 18 locations. At each location, we measured B at least three times. We took the average of all measurements at a given milled region (9 or more) as the value of B. This tends to minimize any (local) variation in $B_o$; recall that $B = B_o + C_A(\sigma_\theta - \sigma_r)$.

Values of B thus obtained are in good agreement with PZT values. Note that the PZT values are usually lower than EMAT values; this "d.c. shift" is due to the difference in the way arrival times are measured with the two different transducers. Furthermore, the shift is about same as the difference in $B_o$ as measured with the EMAT and the PZT transducer.

Stress Measurement

Since we were able to measure $B_o$ for the wheel (due to the sawcut), we can convert the birefringence measurements to stress. We used the same value of the stress-acoustic constant, $C_A = -7.6(10^{-6})/MPa$, that was used in Refs. 1,2 and subtracted $B_o$ from B to obtain $\sigma_\theta - \sigma_r$; see equation (6). The results obtained are shown in Fig. 7 for EMAT and PZT.

There are several interesting features about this figure. First, notice that the peak stress occurs at 180° circumferentially around the wheel from the sawcuts. This is in qualitative agreement with results obtained by researchers at the Transportation Test Center [8]. They found that sawcutting relieved the stress near the cut, but left the stress 180° from the cut almost unchanged.

The second interesting feature about Fig. 7 is the good agreement between EMAT and PZT results. In fact, the difference of peak stress as measured with the different transducers in less than 10 MPa. This agreement shows that there was indeed a constant difference in birefringence measurements between PZT and EMAT; since we subtract $B-B_o$ to obtain $\sigma_\theta - \sigma_r$, the differences cancel out.

A third feature of note is that the EMAT results are almost symmetric about 180° (the line opposite sawcuts). In fact, if the residual stresses (due to casting and braking), and the degree of texture were homogeneous, then one would expect $\sigma_\theta - \sigma_r$ to display this symmetry (about 180°) after sawcutting. The symmetry of the EMAT results is pleasing, since it does indicate that the residual stresses and the texture were axisymmetric prior to sawcutting. We hope to check this hypothesis of axial symmetry by measurements on an uncut wheel.

For the EMAT, we made measurements not only on the milled regions, but also at other locations where we used various surface preparation treatments. At some locations, we merely removed a layer of rust with abrasive paper leaving a surface consisting of both bright metal and pits. At other locations, we used a handgrinder followed by hand sanding with abrasive paper; the resulting surface was smoother, but still contained pits. At other locations, we used only abrasive paper, but sanded for a longer time than when merely removing rust; the surface finish was intermediate between rust-removed surfaces and surfaces cleaned with a handgrinder.

The results obtained using the EMAT on these various surfaces are indicated by different symbols in Fig. 7. Qualitatively, it appears that the degree of surface preparations is not particularly significant as far as EMAT measurements are concerned. For instance, the EMAT data from 0° to 90° agrees quite well with PZT data, except for two points which are off the PZT curve; however, even these points are only off by 25 MPa. For 180° to 360°, the EMAT data is, as mentioned above, approximately the mirror image of the data from 0° to 180° (symmetry about the 180° line).

Recall that we expected systematic errors $\delta t_\theta$, $\delta t_r$ in PZT measurements of arrival times. The effect of these errors appears to have cancelled out in taking the difference $B - B_o$ to obtain stresses, since EMAT and PZT measurements of $\sigma_\theta - \sigma_r$ are in good agreement.

## CONCLUSIONS

We have developed a simple time-interval-averaging system which allows us to measure arrival times with a precision of ± 1 ns or better, using SH-waves propagating through the rim of a cast steel railroad wheel. This

precision was obtained with a PZT transducer and also with an EMAT, both operated in the pulse-echo mode.

We used our EMAT to measure the variation in arrival times on regions next to the sawcut in our wheel. For these cases, the hoop stress (assumed much larger than the radial stress) vanished, so differences in arrival times are due to texture induced by casting the wheel. We found that when the SH-wave was polarized in the radial direction, it had the fastest arrival time; the slowest arrival time occurred for polarization in the circumferential direction. Furthermore, the arrival time displayed an approximately sinusoidal variation with polarization angle. This satisfies a necessary condition for the wheel texture (averaged through the rim thickness) to be orthotropic. The material symmetry axes for the rim appear to be oriented in the thickness, radial, and circumferential direction.

This allows us to use the current theories of acoustoelasticity, which assume orthotropic symmetry [3,4]. The birefringence is related to stress through equation (3); the angle $\phi$ between pure-mode polarization directions (acoustic axes) and the material symmetry axes is related to stress through equation (2).

We measured the angular variation of arrival time at a stressed location and again found that the fastest and slowest arrival times occurred for SH-waves polarized along the radial and circumferential directions, respectively. Since the acoustic axes still correspond to the material symmetry directions ($\phi = 0$), equation (2) shows that there is no shear stress ($\sigma_{r\theta} = 0$). The relation between birefringence and stress can be simplified to

$$B - B_o = C_A(\sigma_\theta - \sigma_r). \qquad (6)$$

In order to obtain the hoop stress $\sigma_\theta$ (assuming negligible $\sigma_r$), we must first obtain the unstressed birefringence (which is due to casting-induced texture). We were able to do this for the sawcut wheel by measuring the birefringence on either side of the sawcuts (locations 1 and 2). We did this with both the EMAT and PZT transducer; we found a small difference (about $1.0(10^{-4})$) in $B_o$ as measured by the two transducers.

We measured the birefringence at different locations around the circumference of the wheel. In order to avoid damage to the PZT transducer, we had certain regions of the rim milled and then hand-polished. We measured B at these regions (1-6) with both types of transducers and found that the EMAT values were usually slightly larger than the PZT values (about $1.0(10^{-4})$).

We also measured B at other locations with just the EMAT. The rim was subjected to various kinds of surface preparation at these locations. We did this so that we might characterize the relation between quality of EMAT measurements and degree of surface preparation.

Finally, we converted our values of $B - B_o$ to hoop stress, and compared EMAT and PZT results. We found that the peak stress occurred at the 180° position (opposite the sawcuts), as expected. The peak stress as obtained by the EMAT was within 10 MPa of the stress obtained by the PZT transducer. We also obtained good agreement at the other milled locations as well.

The stress displayed a high degree of symmetry about the 180° position, indicating that the texture is axisymmetric, and that the hoop stress was axisymmetric before sawcutting. The EMAT results also indicated reliable measurements of B could be obtained with minimal amounts of surface preparation, e.g., using a handgrinder.

The good agreement between EMAT and PZT results indicates that in field applications, the former can be used instead of the latter. This is important, since the EMAT requires less surface preparation, operates with a simpler mounting fixture, needs no couplant, and can be easily scanned and rotated. Some of the disadvantages of the EMAT (such as poor signal-noise ratio) have been overcome with our system, which uses carefully matched electronics to minimize noise. Furthermore, the time-interval averaging feature of our velocity measurement system allows us to operate in an r.f. environment which approximates conditions in the field.

Clearly, much remains to be done in the future. We hope to make additional measurements on uncut wheels to determine, for example, whether the stress and texture are axisymmetric. We also will measure the birefringence as a function of radial position. We hope to develop a method of determining $B_o$ on uncut wheels, and, finally, to determine $\sigma_\theta$ by ultrasonic results.

ACKNOWLEDGMENTS

The work was supported by the Federal Railroad Administration, Department of Transportation, under the supervision of Claire Orth, Research Manager. We were greatly assisted by the generous cooperation of Mr. Britto Rajkumar of the American Association of Railroads, who provided both the wheel and encouragement.

REFERENCES

1. Fukuoka, H., Toda, H., Hirakawa, K., Sakamoto, H., and Toya, Y., "Nondestructive Assessments of Residual stresses in Railroad Wheel Rim by Acoustoelasticity," to be published in J. of Eng. for Industry, ASME.

2. Fukuoka, H., Toda, H., Hirakowa, K., Sakamoto, H., and Toya, Y., "Acoustoelastic Measurements of Residual Stresses in the Rim of Railroad Wheels," in Wave Propagation in Inhomogeneous Media and Ultrasonic Nondestructive Evaluation, G.C.Johnson, ed., AMD-Vol.6 (Published by ASME, 1984).

3. Iwashimizu, Y., and Kubomura, K., "Stress-Induced Rotation of Polarization Directions in Slightly Anisotropic Materials," Int. J. Solids Structures, Vol. 9, 1973, pp. 99-114.

4. Okada, K., "Stress-Acoustic Relations for Stress Measurements by Ultrasonic Techniques," J. Acoust. Soc. Japan (E), Vol. 1, No. 3, 1980, pp. 193-200.

5. Association of American Railroad Specification. Interchange Rule 41.

6. Frost, H. M., "Electromagnetic-Ultrasound Transducer: Principles, Practice, and Applications," Physical Acoustics, Vol. XIV, Mason, W. P., and Thurston, R. N., eds., Academic Press, New York, 1979.

7. Jackson, C. W., "Characterization of Stressed Metals Using Acoustic Shear Waves," Ph.D. Dissertation, Stanford Univ., June 1984.

8. Rajkumar, B., private communication.

9. Clark, A. V., Moulder, J. C., "Residual Stress Determination in Aluminum using Electromagnetic Acoustic Transducers," Ultrasonics, Vol. 23, No. 6, pp. 253-259.

APPENDIX

EMATs have a relatively low signal/noise ratio. Consequently, our time-interval probes will often trigger (generate a square-wave pulse) on noise as well as on the zero crossings in the echo. It is necessary to reject these spurious pulses when measuring arrival times.

On thin aluminum plates, we had found that using an analog gate was a satisfactory solution [9]. However, this solution was found to be unsatisfactory for thick steel sections such as the rim.

We therefore adopted the following approach. Rather than gate out the echo and send the gated signal to the probe, we simply gated out the desired probe pulses from the undesired pulses. (The former pulses, of course, correspond to zero crossings in the echo, and the latter to noise.) The gating was accomplished using digital logic circuits, rather than analog circuits. This resulted in less signal distortion (to avoid changing the apparent arrival time).

The circuits (shown in Fig. 8) work as follows. Voltages from the probes were ocnverted from the range -0.5 V to +0.5 V to digital logic circuit levels (TTL) by using a fast preamplifier/level shifter. The preamplifier had a typical rise time of about 6 ns so that it could follow the rapid rise times of the probe pulses. After a time delay (which we can vary), a "one-shot" device is triggered. This causes the voltage on one terminal of a logic gate (AND gate) to be at logical level "1" (+ 5 volts). The signal from the preamplifier is input to the other gate terminal. When the probe generates the leading edge of a square wave pulse, (and the preamplifier correspondingly generates the leading edge of a TTL pulse) both

terminals of the AND gate will be at logical level "1" and the gate output will also be at logical level "1" (5 volts). When the probe generates the falling edge of the square-wave pulse, the gate output returns to logical level "0" (zero volts). Consequently, the AND gate output essentially replicates the probe pulses.

The gate output goes to the STOP channel of the counter. The trigger level of the counter can be set to stop the counter when it receives a voltage anywhere in the level - 5 to + 5 volts. We adjusted the trigger level to obtain the optimum precision (better then ±1 ns) in arrival times.

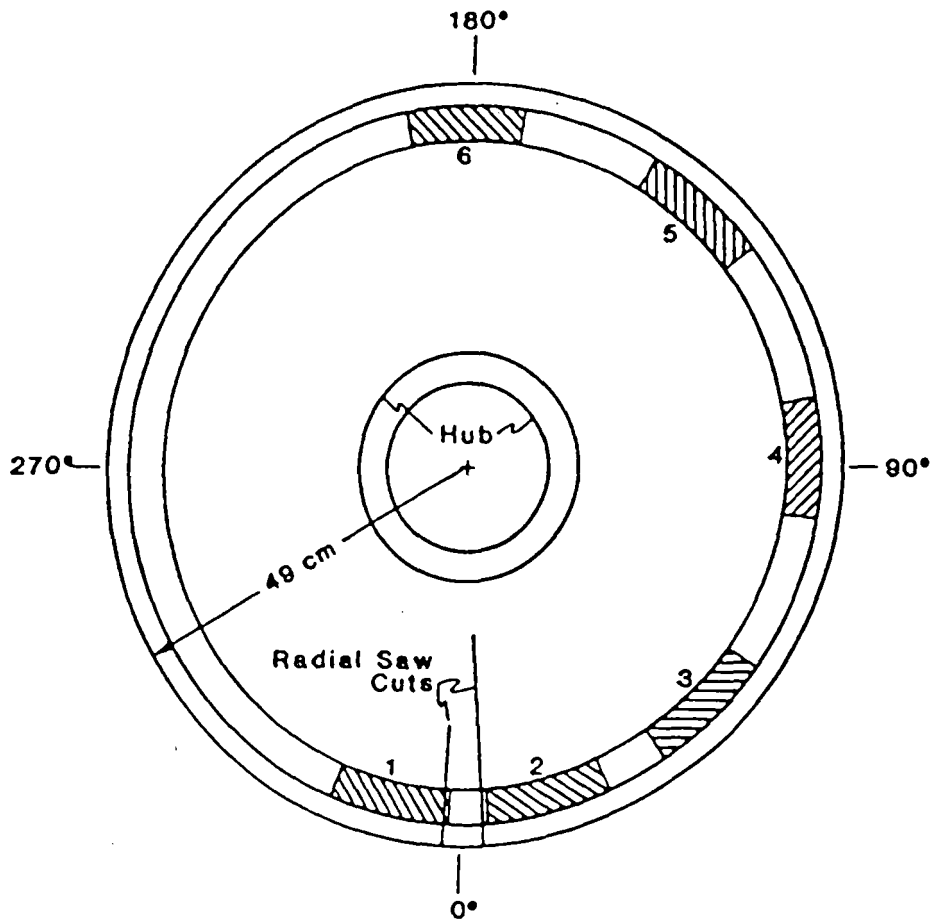


**Figure 1** Top view of the sawcut wheel used in the experiments. Shading indicates milled regions 1–6. Angle $\theta$ is measured circumferentially around the rim from the midpoint of the sawcuts, in an anticlockwise direction

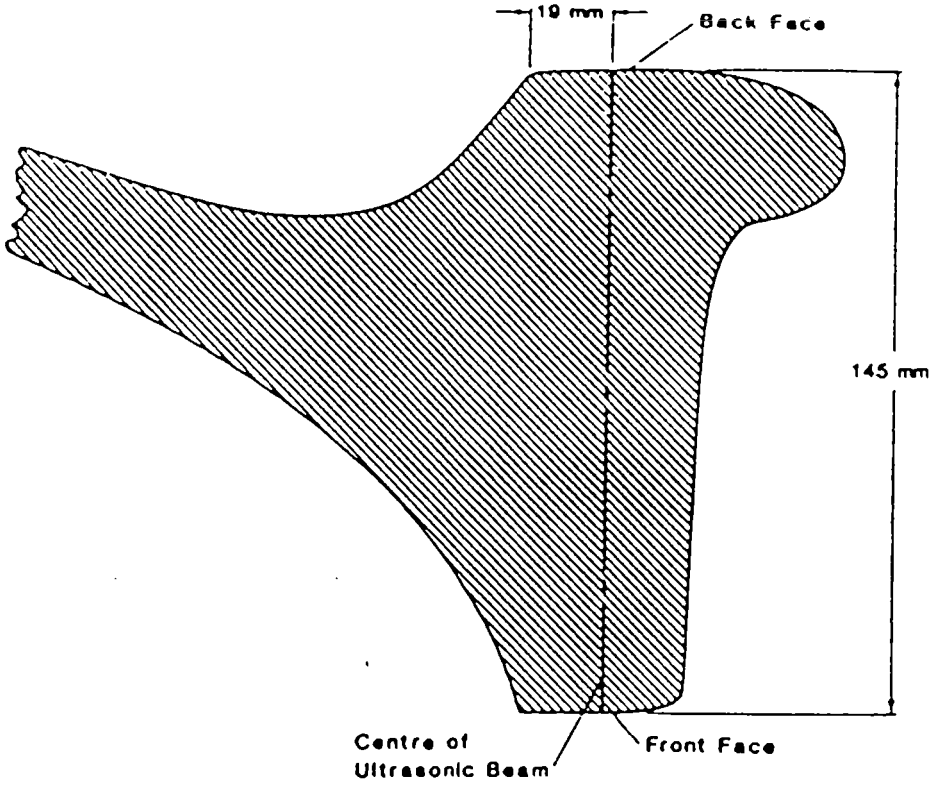


Figure 2 Cross-section of the wheel in the vicinity of the rim. Transducers were placed on the back face of the rim, 19 mm radially outward from the (inner) edge of the rim

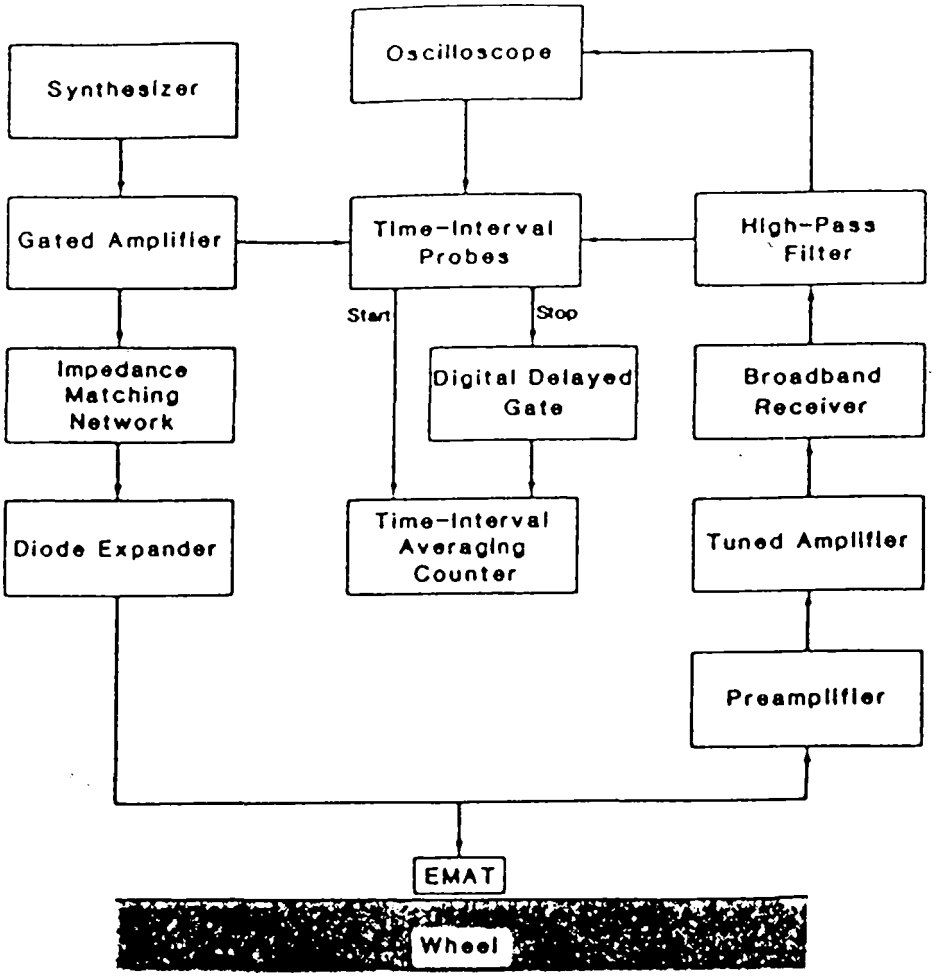


Figure 3 Time-interval averaging system used for EMAT measurements

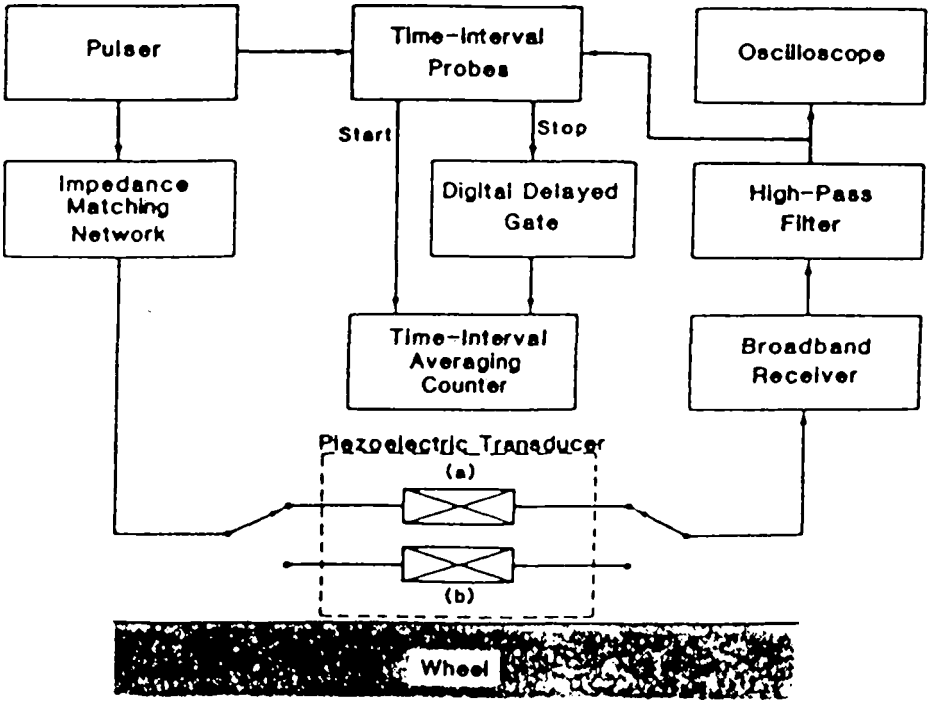


Figure 4 Time-interval averaging system used for PZT transducer measurements. (a) Upper transducer; (b) lower transducer

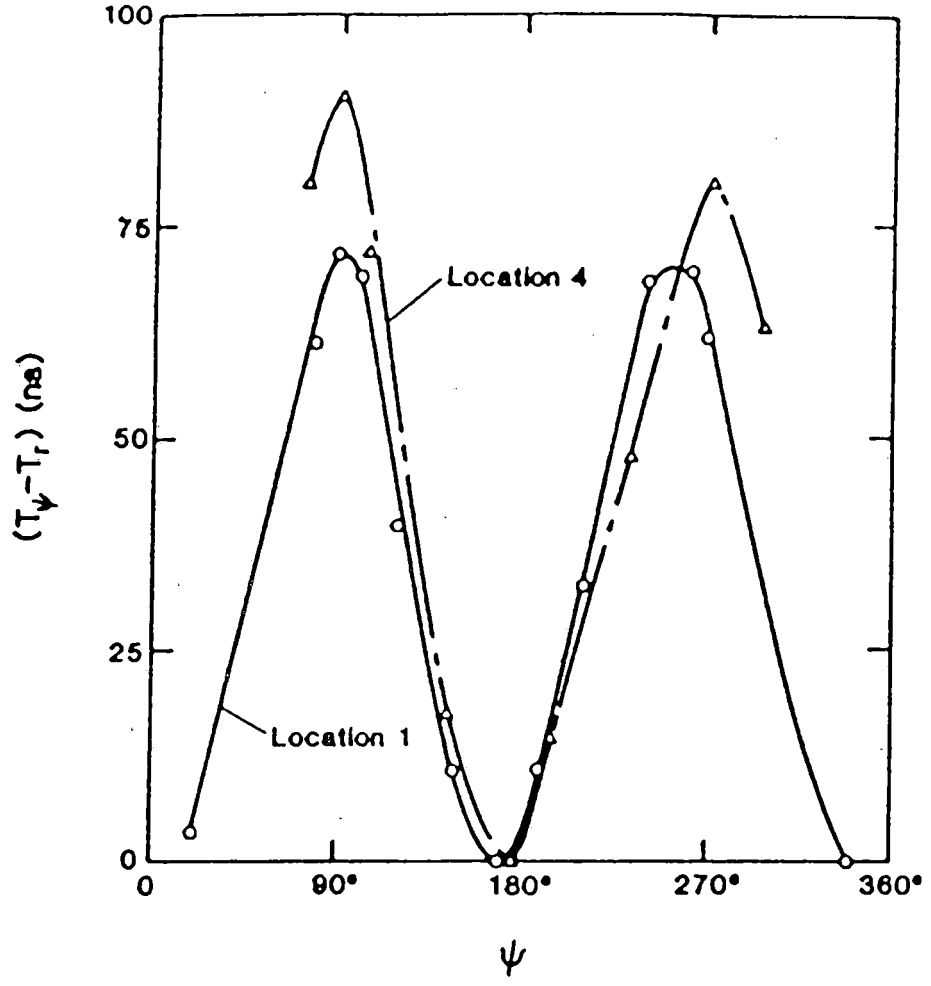


**Figure 5** Angular variation of arrival times for unstressed region (——) and stressed region (— - —) of sawcut wheel. Angle $\psi$ is measured anticlockwise; $\psi = 0°$, 180° when measuring $T_r$; $\psi = 90°$, 270° when measuring $T_H$

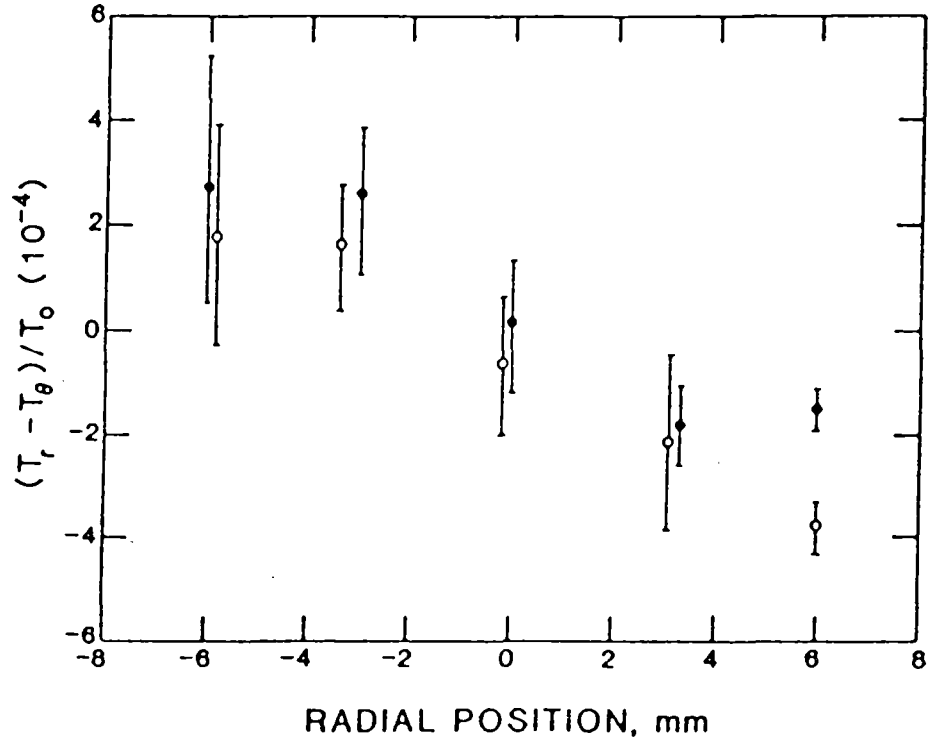


**Figure 6** Birefringence measurements made on rim of sawcut wheel, using both the EMAT (O) and PZT (●) transducer

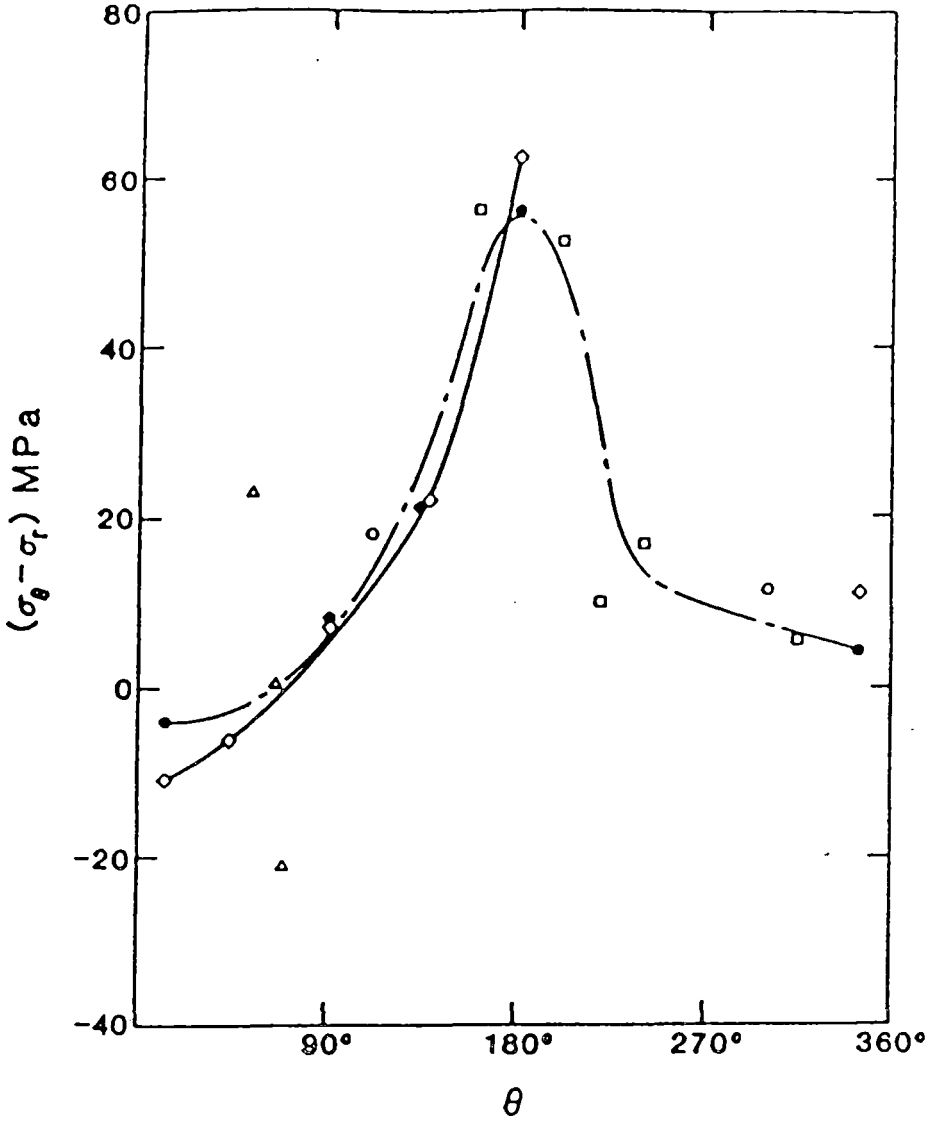


Figure 7 Differences in principal stresses measured on the rim of the sawcut wheel, using both the EMAT and PZT transducer. The EMAT measurements were made using a variety of surface preparations: ●, milled; ○, rust removed; △, hand sanded; □, hand ground and hand sanded. ◇, PZT, milled and hand sanded

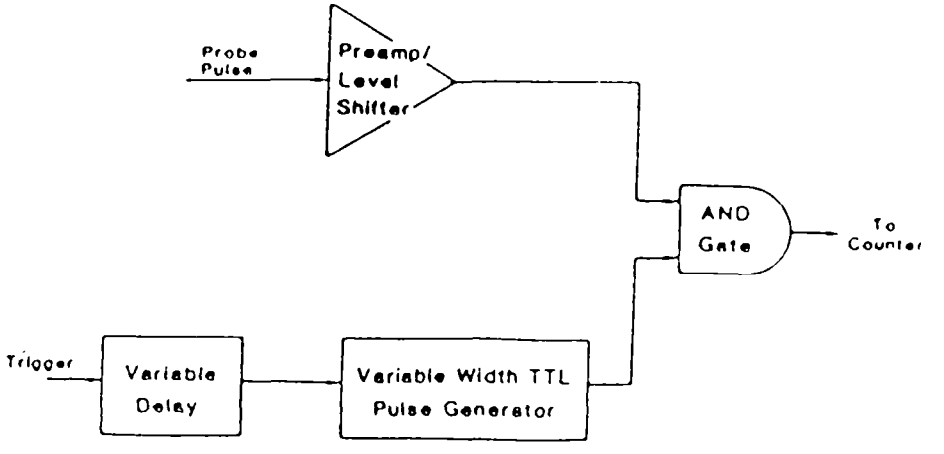


Figure 8 Block diagram of digital delay gate

**Characterization of Residual Stress and Texture in Cast Steel Railroad Wheels**, 1987
AV Clark, jr., H Fukuoka, DV Mitrakovic, JC Moulder